WYATT TECHNOLOGY

Application Note

Coupling MALS and SAXS for time-resolved studies of biopolymeric filamentous networks assembly: fibrin formation

Mattia Rocco, IRCCS AOU San Martino-IST, Genova, IT†

Summary

Multi-angle light scattering (MALS) is primarily used to determine molecular weight, size- and shape-related parameters of macromolecules or nanoparticles as they elute from a separation device. In batch (unfractionated) mode, MALS provides the weight-average molecular weight $<M>_w$ and the z-average mean square radius $<R_g^2>_z$. The **DAWN® HELEOS® II** is particularly well suited for these tasks owing to its flow cell design, holding a mere ~67 µl and readily connecting to a fluid line through HPLC-type fittings. This very same design can be used profitably to study a sample evolving in time, such as a polymerization or degradation reaction, by injecting a sample into the flow cell with a stopped-flow apparatus.

Small-angle X-ray scattering (SAXS) is a powerful technique that also measures $<M>_w$ and $<R_g^2>_z$. SAXS accesses much shorter length scales than does MALS, such as the low-nm cross-sections $<R_c^2>_z$ of elongated solutes. MALS and SAXS are therefore complementary techniques for determining valuable structural information, especially when applied to evolving samples.

This Application Note describes measurements made using a stopped-flow MALS-SAXS set-up that was implemented at the **SWING** beamline of the **SOLEIL** synchrotron near Paris, France. The apparatus was developed for the study of the formation of fibrin networks following enzymatic activation of fibrinogen molecules. In this reaction, central to the blood coagulation system, rod-like macromolecular monomers ~47 nm long rapidly assemble into branched fibers 100-200 nm thick and spanning many microns (top image, right). The SAXS-MALS set-up has produced data of excellent quality (bottom image, right), providing compelling evidence that led to a profound revision of the standard model of fibrin polymerization.

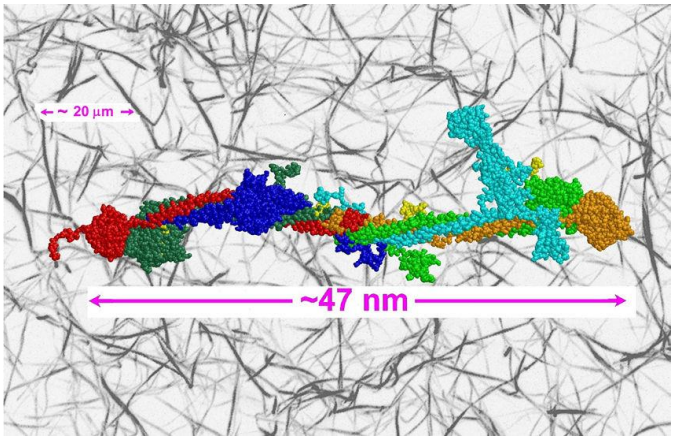

An atomic model of fibrinogen superimposed on a confocal microscopy image of a fibrin network. The approximate dimensions given highlight the ~500-fold change in the characteristic length scale following polymerization.

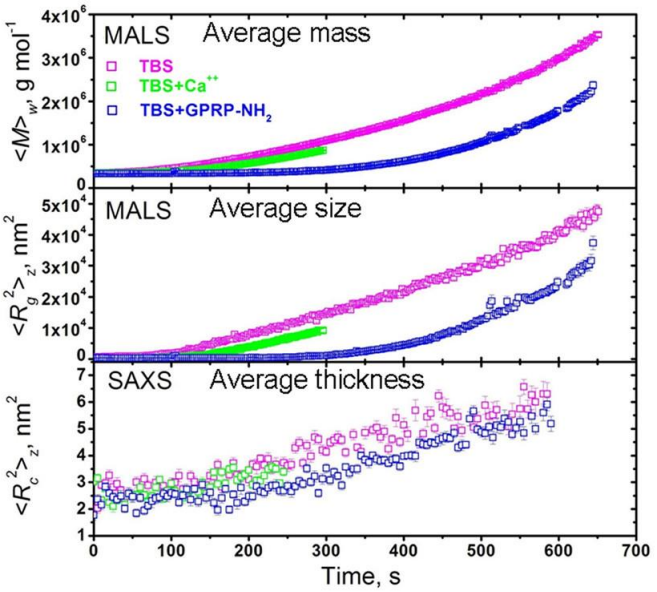

Coupled MALS/SAXS measurements of activated fibrinogen polymerization under different conditions. SAXS provides the thickness of the fibrils while MALS provides a measure of size dominated by the length of the fibrils. Credit: see footnote *

†mattia.rocco@hsanmartino.it

I. Introduction

Biopolymeric filamentous networks are key components in the living world. Prime examples are the cell cytoskeleton (actin), the connective tissue (collagen), and the blood coagulation system (fibrin). Since they result from the assembly/polymerization of macromolecular monomers, these processes can be studied with time-resolved scattering techniques initiated upon combining pure components.

The use of a DAWN DSP MALS instrument was described previously for studying the early stages of the fibrinogen (FG) assembly after enzymatic activation, recovering the time evolution of the $<R_g^2>_z$ and $<M>_w$ of the ensembles [1,2]. However, the evolution of an important structural parameter in fibrous structures formation, the fiber cross-section, cannot generally be recovered in the early reaction stages from MALS data. Potentially the so-called "Casassa plot" method could determine the fiber cross-section, but usually the vast majority of the reactant species are too short (<200 nm) to allow its application [3]. The cross-sectional mean square radius $<R_c^2>_z$ can instead by recovered from SAXS data [4].

An experimental set-up comprising a stopped-flow mixer, a Peltier-equipped **HELEOS-II** 18-angles MALS detector, and a SAXS flow-through capillary cell, has been assembled at the **SWING** beamline of the synchrotron **SOLEIL** (Gif-sur-Yvette, France). This set-up, where the MALS detector plays a central role, enabled us to follow the coupled evolution of $<R_g^2>_z$ *vs.* $<M>_w$ and of $<R_c^2>_z$ *vs.* $<M>_w$ during the early phases of fibrin polymerization.

Modeling of possible reaction pathways revealed that the classical mechanism of fibrin assembly, involving the immediate formation of fully double-stranded fibrils with a half-staggered arrangement of monomer units (Fig. 1), was inadequate to describe the data. A revised model was thus proposed that not only is fully compatible with the data, but could also explain several other features of the fibrin network [5].

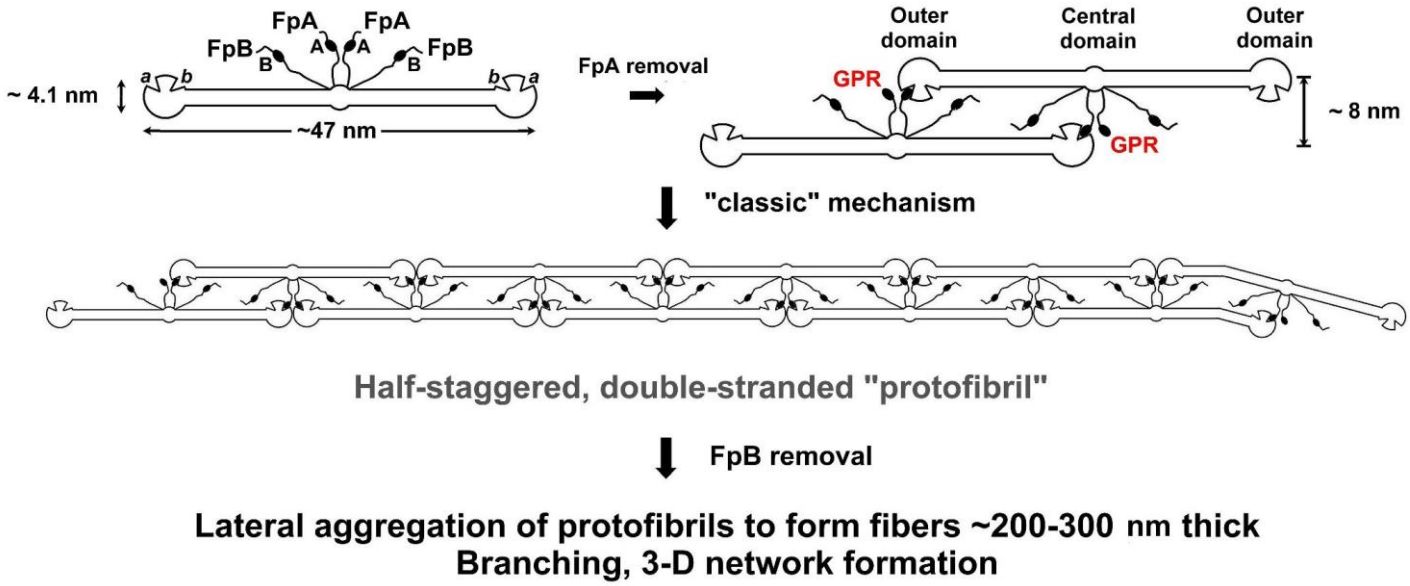

Figure 1: The "classical" model for fibrinogen network formation. Following enzymatic removal of two short peptides (FpA) from the central domain of FG molecules, Gly-Pro-Arg (GPR) "knobs" are uncovered, which are complementary to "holes" always present in the outer domains of every FG molecule. This initiates self-assembly, producing long, half-staggered, fully double-stranded (proto)fibrils. Lateral fibril aggregation and branching aided by delayed enzymatic removal of another pair of peptides (FpB) generate the final fibrin network. Credit: see footnote*

II. Materials and Methods

Reagents

All chemicals were reagent grade (Merck, VWR International, Milano, IT). MilliQ water was used for all the solutions. Lyophilized, plasminogen-depleted human FG was from ERL (South Bend, IN, USA). It was reconstituted at 20 mg/ml and purified over a preparative size-exclusion column right before experiments to yield ~20 ml at ~2 mg/ml stock solutions. The activating enzyme Ancrod (from snake venom) was A-5042 from Sigma-Aldrich. Vials with 50 NIH units/ml aliquots were prepared and stored at -80 °C. GPRP-NH_2 was H-1998 from Bachem (Bubendorf, CH). The buffer used in all experiments was Tris 50 mM, NaCl 104 mM, aprotinin 10 KIU/mL, pH 7.4 (TBS), without or with $CaCl_2$ 1.25 mM.

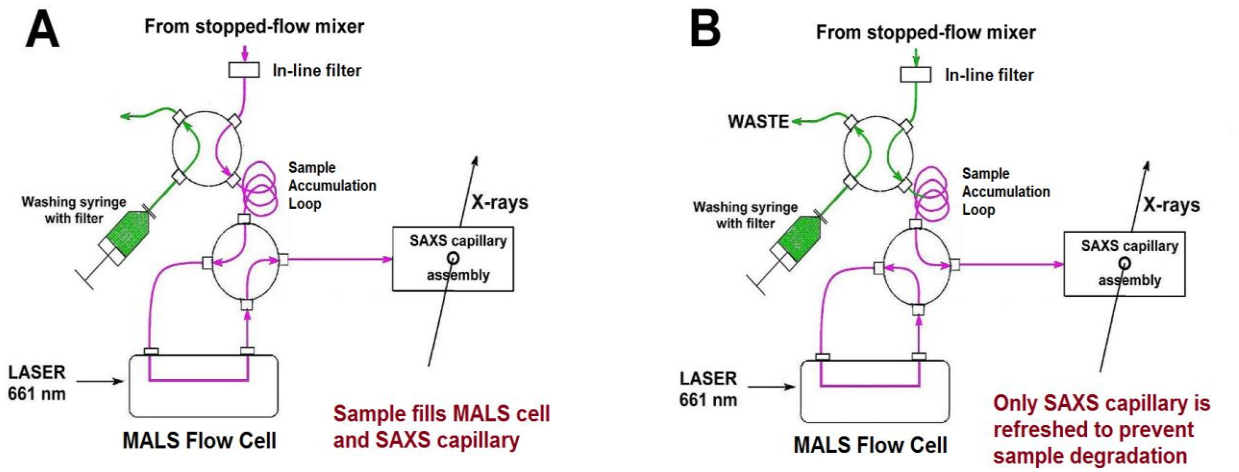

Figure 2. Schematic diagram of the stopped-flow MALS/SAXS set-up. Two positions of the lower valve are shown; other valve combinations are used during an experiment (see [5]). Green, buffer; magenta, reacting mixture. Credit: see footnote*

Instrumentation

SAXS beamline measurements require apparatus to be remotely-controlled (Figs. 2-3). The set-up included a four-syringe, stopped-flow mixer (SFM4, Bio-Logic, Grenoble, FR) modified with the addition of external solenoid valves, a mixer, and a splitter. This arrangement avoids cross-contamination during the long waiting times between injections (up to 10 min and more), and allows immediate flushing of the external mixer after the injection is complete. An in-line, 70 µL PEEK/titanium 0.1 µm filter housing (WTC #2713) is placed right after the mixer to remove particulates.

While the reaction mixture should be left undisturbed inside the MALS cell for time-resolved measurements, it must be "refreshed" regularly while in the SAXS capillary so as to prevent irreversible damage to the protein by the intense X-ray beam. A four-way rotary valve placed between the MALS and the SAXS cells isolated the MALS cell right after injection, directing flow to the SAXS capillary (Figs. 2-3). Solution was pushed through the SAXS capillary in 5 µl increments every two X-ray shots, each one lasting 0.5 s with a 5 s interval. About 1.6 ml were required to completely fill both cells and the accumulation loop.

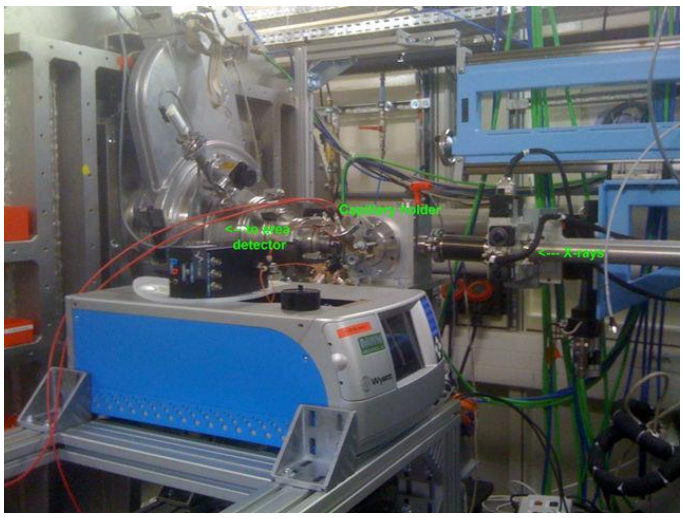

Figure 3. The combined MALS-SAXS apparatus in the SWING beamline hutch at SOLEIL.

*Reprinted and/or adapted with permission from Rocco et al, "A Comprehensive Mechanism of Fibrin Network Formation Involving Early Branching and Delayed Single- to Double-Strand Transition from Coupled Time-Resolved X-ray/Light-Scattering Detection" *J. Am. Chem. Soc.* 2014, **136**, 5376-5385 and Supporting Information. Copyright 2014 American Chemical Society.

MALS data acquisition and analysis

To mitigate laser-heating of the static MALS sample, the HELEOS-II cell was maintained at 20±0.1 °C. Data acquisition and initial analysis was performed with the **ASTRA**® 6.0.3 software. A *dn/dc* value of 0.192 cm^3/g was used for FG. For TBS, n=1.3332 at λ=651 nm, making 16 scattering angles available, from 13.5° to 157.5°. The QELS fiber optic was placed in position #12 at ~100°. Normalization was performed using the R_g of FG directly measured by SAXS on the very same sample. More than one polymerization run was usually acquired in the same file, with buffer-mixture-buffer sequences directly injected while ASTRA was running. An example of a partially processed run is shown in Fig. 4.

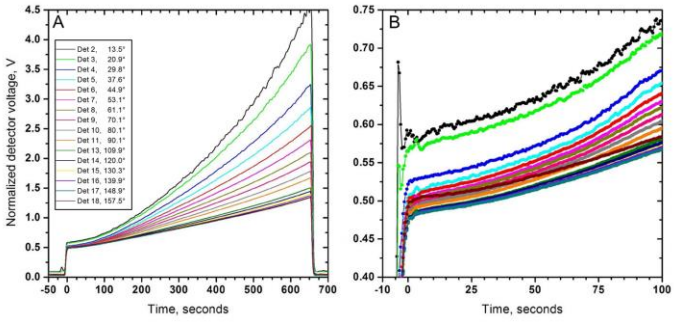

Figure 4. Angular MALS data (normalized voltages) collected by a HELEOS-II from a 0.46 mg/ml fibrinogen (FG) sample undergoing polymerization induced by 0.05 NIH units/mg FG of the snake venom enzyme "Ancrod". The reaction was stopped before the gel point. Panel A, complete dataset. Panel B, the first ~100 s on an enlarged scale. Times are rescaled to the end of the injection phase. Note the excellent quality of data even at the lowest angles. Credit: see footnote*

The data were processed using the Zimm formalism. Since the reaction produces a heavily polydisperse mixture of rod-like species, the Zimm plots rapidly deviate from angular linearity (see Fig. 5). Each dataset was therefore fitted with different polynomials from the 1st to the 5th degree, including and excluding the two lowermost angles (see Fig. 5). The resulting $\langle R_g^2 \rangle_z$ and $\langle M \rangle_w$ datasets were then exported to an Excel® spreadsheet to manually "collate" sections for optimal fitting of angular dependence to determine $\langle R_g^2 \rangle_z$ values ($\langle M \rangle_w$ values being less influenced by the specific fitting procedure).

Extensive simulations were conducted to ascertain that this procedure correctly yields the $\langle R_g^2 \rangle_z$ values of polydisperse ensembles of rod-like particles (see [5] for details).

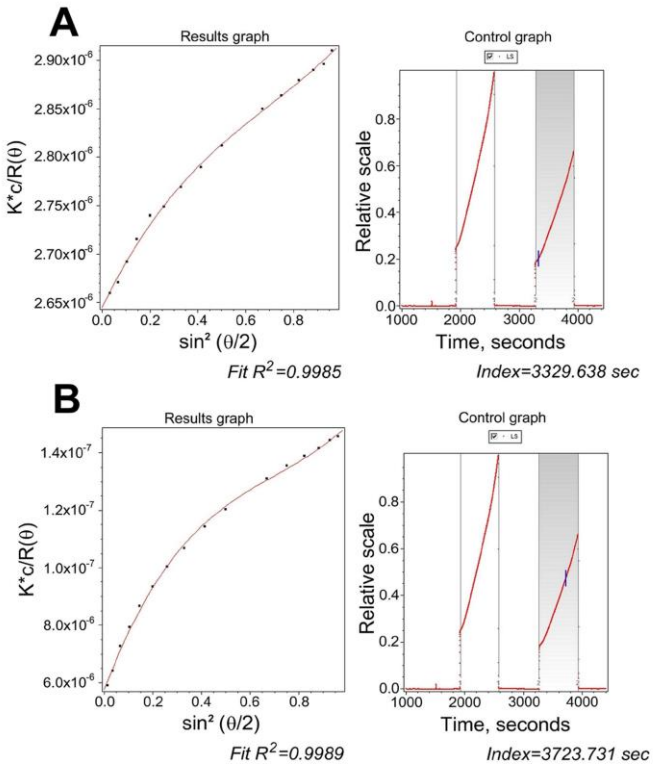

Figure 5. ASTRA processing of the data from Fig. 4. Panel A, a slice collected at 51 s after mixing, highlighting the need for no less than a 3rd degree polynomial and for including the 20.9° scattering angle. Panel B, a slice collected at 445 s after mixing, where a 5th degree polynomial was required using all angles. Credit: see footnote*

SAXS data acquisition and analysis

The SWING beamline technical specifications can be found in [6]. The SAXS detector distance was 4 m for the non-polymerizing FG runs (momentum transfer q of $0.0032<q<0.18$ Å^{-1}; $q=4\pi \sin(\theta/2)/\lambda$, θ is the scattering angle and λ=1.033 Å the X-ray wavelength). For the polymerization runs, the distance was 2 m ($0.00568<q<0.5$ Å^{-1}). After in-house data treatment, $\langle R_c^2 \rangle_z$ values were derived from cross-section Guinier plots [4] with the **US-SOMO** SAS module [7].

Modeling

A detailed description of the complex fibrin polymerization modeling, which utilizes a modified Flory bifunctional polycondensation scheme and represents each FG unit as a cylinder, can be found in [5]. Significantly, the modeling allows accounting for the ratio of release Q between the two FpA from a single FG molecule (see Fig. 1). High Q values produce distributions skewed toward long polymers.

III. Results and Discussion

A series of datasets plotting the mean square radius, $\langle R_g^2 \rangle_z$, weight-average molar mass, $\langle M \rangle_w$, and mean-square thickness $\langle R_c^2 \rangle_z$ *vs*. time is shown in Figure 6 for FG polymerizations induced by Ancrod under different solvent conditions: TBS, TBS + $CaCl_2$ 1.25 mM, TBS + GPRP-NH_2 in a 10-fold molar excess to FG. Note the large differences between the three conditions in the time evolution of $\langle R_g^2 \rangle_z$ and $\langle M \rangle_w$, while only a slight difference in the $\langle R_c^2 \rangle_z$ data is apparent when the GPRP-NH_2 inhibitor is present as opposed to no GPRP-NH_2.

However, when the time factor is removed from the same data by plotting $\langle R_g^2 \rangle_z$ *vs.* $\langle M \rangle_w$, as shown in Fig. 7A, the three datasets nicely superimpose on each other, revealing that the basic polymerization mechanism is the same, notwithstanding the large differences in the time evolution. A relatively small difference is present in the $\langle R_c^2 \rangle_z$ *vs.* $\langle M \rangle_w$ plot when the GPRP-NH_2 inhibitor is present in rate-limiting quantities (Fig. 7B).

Modeling was then done to interpret the results. First, the classic model (see Fig. 1) was employed. Fully half-staggered, rod-like double-stranded (RLDS) rigid polymers were able to fit only the initial portion of the $\langle R_g^2 \rangle_z$ *vs.* $\langle M \rangle_w$ plots (Fig. 6A, grey dashed curve). Fully half-staggered, worm-like double stranded (WLDS) semi-flexible polymers fit the entire $\langle R_g^2 \rangle_z$ *vs.* $\langle M \rangle_w$ datasets (Fig. 7A, orange dashed curve). However, **neither** of these models could fit the $\langle R_c^2 \rangle_z$ *vs.* $\langle M \rangle_w$ curves (Fig. 7B, dashed grey curves), revealing that the thickness of the polymers increases more slowly than that predicted by the classic model!

A new fibrin polymerization model was then devised. It involves a single binding event and a delayed transition to the fully double-stranded (DS) fibrils (Fig. 8A). This elongation mode not only produces polymers whose R_g is very close to that of their corresponding fully DS entities, but also whose cross-section as seen by SAXS is the same as that of the parent FG monomers. Moreover, the new model allows branches to start growing at a very early stage (Fig. 8B). By fine-tuning the branching occurrence and the DS transition, model curves fitting **both** the entire $\langle R_g^2 \rangle_z$ *vs.* $\langle M \rangle_w$ and $\langle R_c^2 \rangle_z$ *vs.* $\langle M \rangle_w$ plots were generated (Fig. 7, black lines). See [5] for additional details of the modeling procedures.

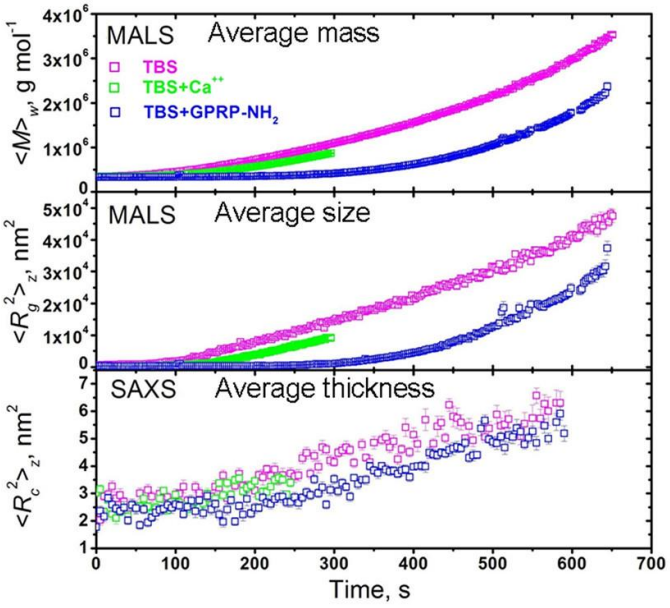

Figure 6. Coupled MALS/SAXS measurements of activated fibrinogen polymerization under various conditions: TBS, is a Tris saline buffer; TBS with Ca^{++}; and TBS with GPRP-NH_2, a peptide that competes for the binding sites, used in rate-limiting amounts. Reactions were stopped before the gel point, which occurs earlier with Ca^{++}. Credit: see footnote*

*Reprinted and/or adapted with permission from Rocco et al, "A Comprehensive Mechanism of Fibrin Network Formation Involving Early Branching and Delayed Single- to Double-Strand Transition from Coupled Time-Resolved X-ray/Light-Scattering Detection" *J. Am. Chem. Soc.* 2014, **136**, 5376-5385 and Supporting Information. Copyright 2014 American Chemical Society.

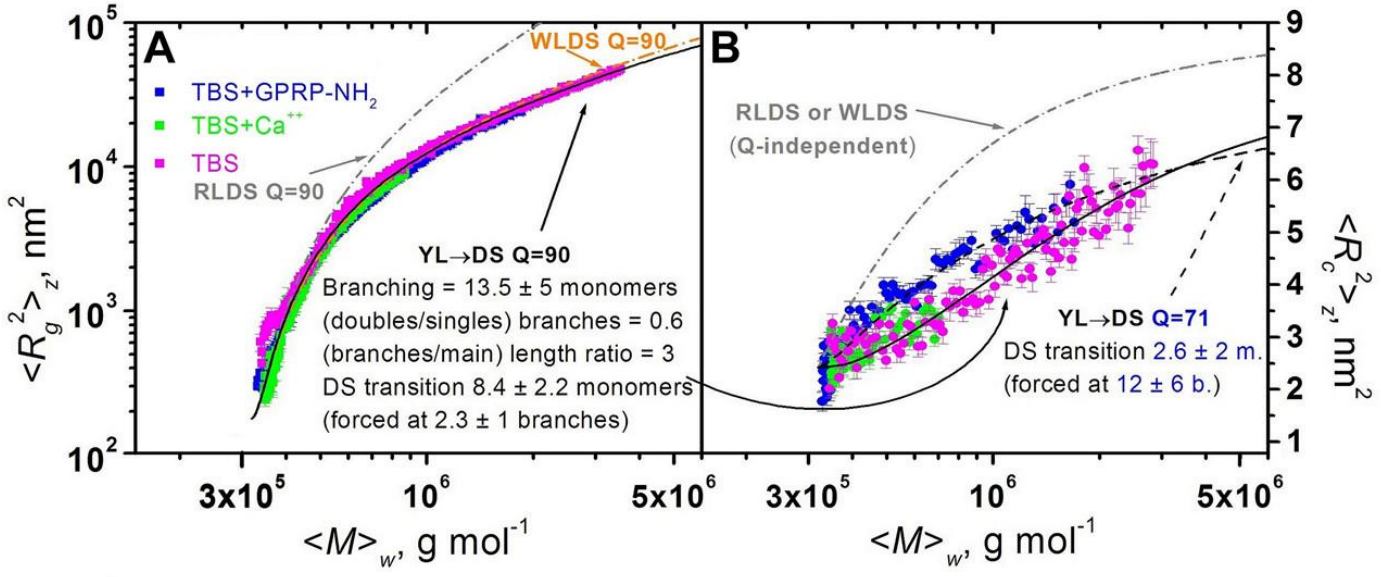

Figure 7. Plots of mean square radius vs. weight-average molar mass (A) and of mean square thickness vs. weight-average molar mass (B) for FG polymerizations under different conditions. Superimposed are model curves generated for some polymerization models (see text). Credit: see footnote*

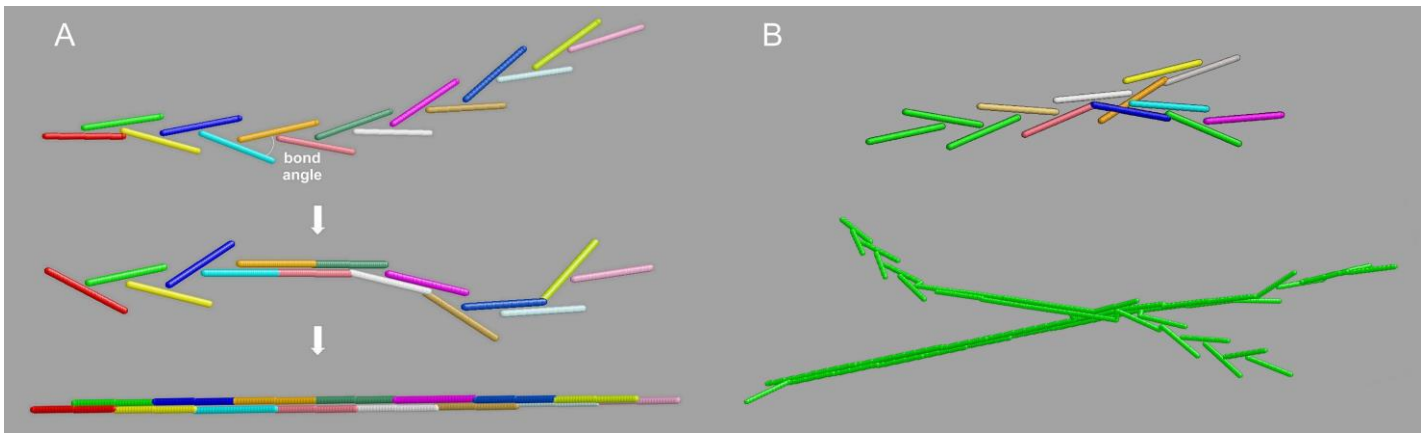

Figure 8. The "Y-ladder to double-stranded" (YL→DS) model for fibrin polymerization. Panel A, the single-binding to full DS transition. Panel B, top: branched structures generation by off-axis binding of a growing chain to a still available A knob; bottom: a typical resulting branched fibril, with the growing ends still in the YL configuration. Credit: see footnote*

IV. Conclusions

In early stages of a polymerization reaction, fibrin networks exhibit formation of elongated, rod-like monomers, later proceeding to the assembly of long fibrils that eventually branch and thicken. MALS measurements are essential to elucidation of this complex behavior. Time-sequenced MALS data establish the evolution of size-and shape-related parameters. The extended angular range and reliable data provided by the temperature-controlled 18-angle DAWN form a solid foundation for the extensive modeling studies required to fully describe such systems.

The addition of simultaneous SAXS data acquired in tandem with MALS, made possible by the DAWN's flow cell configuration, was crucial to establish the lateral growth profile of the fibrils as they thicken and branch.

The commonly-accepted model of fibrin network formation does not allow for branching to take place very early in the polymerization process. The robust results of the MALS-SAXS analysis led us to revise this paradigm with confidence. In the new model, some of the branches in the growing fibrin lumps may, at some point, interconnect, while others collapse on the just-formed main network filaments, giving rise to thicker but low-density fibers [5].

ASTRA software provided advanced capabilities for primary MALS data acquisition and processing. However, due to the highly complex and polydisperse nature of the ensembles of rod-like particles formed in the fibrin polymerization process, additional data treatment was necessary. A manual method to identify the optimal angular range and polynomial order for analyzing non-linear Zimm plots was thus devised. Work is in progress to at least partially automate this task.

In conclusion, the rapid-mixing MALS/SAXS set-up described herein, now a regular user facility at the SOLEIL synchrotron SWING beamline, has produced data of excellent quality. We encourage researchers studying similar reactions, producing filamentous networks either in the biological or synthetic polymers fields, to take advantage of this exciting opportunity, perhaps having first extensively characterized their systems with their own MALS instrument in the comfort of their home laboratory!

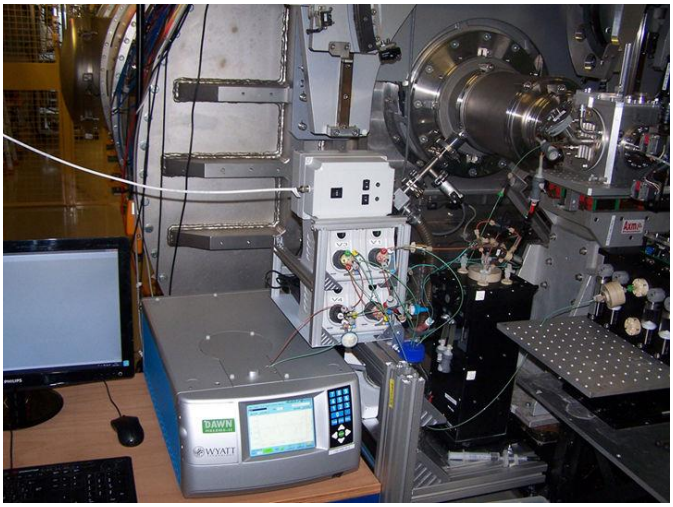

A later version of the stopped-flow MALS-SAXS set-up at the Synchrotron SOLEIL SWING beamline

V. References

[1] Bernocco S., *et al.* 2000. *Biophys. J.* **79**, 561-583.

[2] Rocco M., *et al.* 2001. *Ann. N.Y. Acad. Sci.* **936**, 167-185.

[3] Casassa E. F. 1955. *J. Chem. Phys.* **23**, 596–597.

[4] Glatter O. & Kratky O. 1982. Small-Angle X-ray Scattering. Academic Press, Waltham, MA.

[5] Rocco M, *et al.* 2014. *J. Am. Chem. Soc.* **136**, 5376−5384.

[6] David G. & Pérez J. 2009. *J. Appl. Crystallogr.* **42**, 892−900.

[7] Brookes E, et al. 2013. *J. Appl. Crystallogr.* **46**, 1823−1833.

[8] Janmey P.A. 1982. *Biopolymers* **21**, 2253−2264.

The author would like to acknowledge that this work could not have been done without the efforts of many collaborators, in particular of J. Pérez, P. Vachette, M. Molteni, F. Ferri, B. Cardinali, M. Ponassi, A. Profumo. Thanks are also due to P. Roblin and Y. Liatimi for their work in the current MALS-SAXS implementation.